

RESEARCH

Open Access



# Inflammatory memory-activated biomimetic nanovesicles regulate neutrophil plasticity and metabolic reprogramming for rapid diabetic wound healing via targeting miR-193a-5p/TLR4/JNK/P38 MAPK pathways

Yunlong Fan<sup>1,2†</sup>, Jiaman Yang<sup>3†</sup>, Yulin Xie<sup>3†</sup>, Xin Yang<sup>1</sup>, He Zhu<sup>1</sup>, Yuanyuan Liu<sup>1,2</sup>, Zhikuan Xia<sup>1,2,3\*</sup>, Shuaifei Ji<sup>2\*</sup> and Rongya Yang<sup>1,2,3\*</sup>

## Abstract

Diabetic wound therapy faces significant challenges due to the complexity of the wound microenvironment, especially dysregulated immune cell responses and persistent pro-inflammatory state. Targeting immune cells to reverse pathological wound conditions has increasingly become a promising strategy to promote diabetic wound healing. It has been reported that prolonged memory to acute inflammation sensitizes epidermal stem cells (EpSCs) to tissue damage. The increasing importance of interactions between immune cells and tissue stem cells has raised interest in the potential of EpSCs to induce inflammatory adaptations in diabetic wounds, and meanwhile, the inflammation memory patterns also provide new insight in EpSCs for tissue repair. Here, bioinspired cell-derived mimetic nanovesicles (MNVs) were obtained from inflammation memory-activated EpSCs. LPS treatment could trigger acute inflammation response and activate inflammation memory. MNVs derived from LPS-pretreated EpSCs (LEM) can effectively promote diabetic wound healing by manipulating crucial neutrophil regulatory mechanisms. The *in vitro* and *in vivo* studies demonstrated that LEM could stimulate neutrophil mitochondrial metabolic reprogramming, overcome phenotypic switching deficiency of neutrophils, and skew neutrophils toward N2 anti-inflammatory phenotype via regulating miR-193a-5p/TLR4/ JNK/P38 MAPK pathways in diabetic models. Our findings highlighted the great potential of inflammation memory in EpSCs, and also provided an alternative for diabetic wound treatment.

<sup>†</sup>Yunlong Fan, Jiaman Yang and Yulin Xie contributed equally to this work.

\*Correspondence:

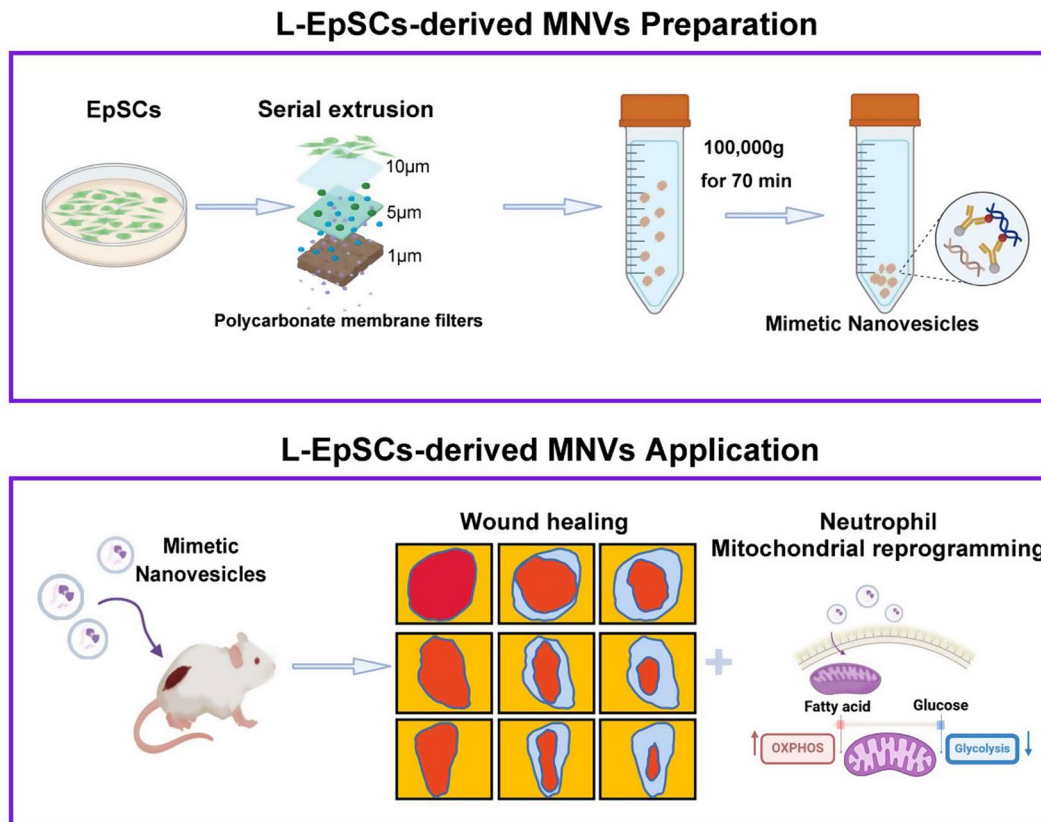
Zhikuan Xia  
sum7@sina.com  
Shuaifei Ji  
jiflyfly301@163.com  
Rongya Yang  
yangrya@sina.com

Full list of author information is available at the end of the article



© The Author(s) 2025. **Open Access** This article is licensed under a Creative Commons Attribution-NonCommercial-NoDerivatives 4.0 International License, which permits any non-commercial use, sharing, distribution and reproduction in any medium or format, as long as you give appropriate credit to the original author(s) and the source, provide a link to the Creative Commons licence, and indicate if you modified the licensed material. You do not have permission under this licence to share adapted material derived from this article or parts of it. The images or other third party material in this article are included in the article's Creative Commons licence, unless indicated otherwise in a credit line to the material. If material is not included in the article's Creative Commons licence and your intended use is not permitted by statutory regulation or exceeds the permitted use, you will need to obtain permission directly from the copyright holder. To view a copy of this licence, visit <http://creativecommons.org/licenses/by-nc-nd/4.0/>.

## Graphic Abstract



**Keywords** Inflammatory memory, Mimetic nanovesicles, Epidermal stem cells, Neutrophils, Diabetic wounds

## Introduction

Chronic wounds, as a common complication of diabetes, pose lifelong risks of developing into diabetic foot ulcers, which put patients at the danger of amputation and impose a great financial burden on patients and the healthcare system [1, 2]. Persistent inflammation and disrupted immunoregulation are the main pathological characteristics of diabetic wounds, and they can initiate a series of harmful effects such as excessive inflammatory cytokines, aggravated reactive oxygen species, increased white blood cell counts, and an elevated risk of bacterial infection, finally leading to delayed wound healing or nonhealing [3]. High levels of glucose and the resulting advanced glycation end products (AGEs) in diabetic wound microenvironments could impair the plasticity of immune cell (e.g. macrophage and neutrophils) and impede the phenotypic transition of macrophage and neutrophils, leading to pro-inflammatory immune cells abounding in diabetic wound [4]. For example, our previous work has reported that inflammation dysregulation observed in diabetic wounds causes more neutrophils infiltrating to the wound but less N2 anti-inflammatory

subtype, leading to prolonged inflammation and poor healing [5]. Then, introducing more N2 neutrophils to the wound site could significantly accelerate the wound healing process and mitigate the excessive inflammatory response [5]. In addition, long-term enrichment of N1 pro-inflammatory subtype neutrophils and inhibition of neutrophil N2 polarization also exhibited exacerbated neutrophil extracellular traps (NETs) activation and release (NETosis), as well as angiogenesis inhibition [6–8], and all these have been reported to greatly hinder diabetic wound healing. These results highlighted the importance of neutrophil phenotypic transition in chronic wound treatment, and restoring neutrophil plasticity may be an effective therapeutic strategy.

EpSCs, as one type of skin epithelial stem cells, are of great importance to skin homeostasis and wound healing. Crosstalk within the epidermal niche between epidermal stem cells (EpSCs) and immune cells is vital for successful cutaneous wound repair [9, 10]. One example is that EpSCs confronting harsh inflammatory environments orchestrate the recruitment of regulatory T (Treg) cells and neutrophils during wound healing [11,

12]. Recent researches described the “inflammatory memory” in EpSCs, and that is, prior exposure to inflammatory mediators results in a quicker and more robust repair response of EpSCs upon subsequent tissue damage [13, 14]. Under inflammatory stimuli, EpSCs sensed and “trained” by environmental assaults, and exhibited enhanced repair ability [13, 15]. Another example of “inflammatory memory” in EpSCs is that temporary exposure of the skin to imiquimod could result in a sudden inflammatory and type 17 immune response, which also enhanced the capacity of EpSCs for tissue repair in subsequent damage [13, 14, 16, 17]. In addition to EpSCs, inflammatory memory also confers healing advantages to other cells, such as corneal epithelial cells [18], mucosal epithelial cells [19], and muscle stem cells [20]. Inflammatory memory-activated epithelial cells have enhanced interactions with immune cells in tissue repair [19]. This unique biological trait that injury experienced EpSCs retained long-term enhanced regenerative ability due to inflammatory memory activation brings new clues for exploring effective treatment of chronic wounds. The therapeutic strategy based on inflammatory memory-activated EpSCs may present a promising to reverse pathological wound conditions and promote healing. However, it has been reported the harsh wound environments could impede the ability of EpSCs to repair the injury [11]. Besides, EpSCs transplantation also faces immunological and ethical concerns. Therefore, there is the need to develop the novel therapeutic strategy independent of cell implantation.

Exosome vesicles (EVs) have exhibited great potential in tissue repair [21]. However, current exploitation of EVs is limited due to time-consuming extraction procedures and low output quantities. Reportedly, the quantity of proteins found in the EVs released by dendritic cells after 24 h of culture can be as little as 500 ng from a million cells [22]. In contrast, cell-derived mimetic nanovesicles (MNVs), which possess biomimetic properties akin to EVs, have attracted increasing attention recently. They can be acquired by extrusion of donor cells. This makes them a potential alternative to address the technical obstacles linked to EVs therapy [23]. Moreover, MNVs can be produced at a significantly reduced cost compared to EVs, amounting to only 10% of the expense. Nevertheless, MNVs have the capacity to produce significantly more material than exosomes, up to 100 times as much in terms of quantity [24]. MNVs have been as the therapeutic application in various diseases [25, 26]. Thus, MNVs derived from inflammatory memory-activated EpSCs have great advantages, and may offer a novel approach to diabetic wound healing.

Here, LPS was utilized to establish inflammatory memory in EpSCs (L-EpSCs) [16]. MNVs from EpSCs with and without LPS pretreatment, also named EpSCs-MNVs

(EM) and L-EpSCs-MNVs (LEM), respectively, were obtained by mechanical extrusion. Our results revealed LEM have the strong ability to restore the plasticity of neutrophils, further reduce inflammation, augment wound cell proliferation, accelerate re-epithelialization, and promote diabetic wound regeneration. Mechanically, LEM achieved high efficient neutrophil phenotypic transition from N1 pro-inflammatory subtype to N2 anti-inflammatory subtype, and reversed persistent pro-inflammatory state in diabetic wounds. Additionally, LEM initiated mitochondrial metabolic recalibration in neutrophils at the wound site by delivering miR-193a-5p and further manipulating TLR4/JNK/P38 MAPK pathways. Comprehensively, LEM drove metabolic reprogramming and phenotypic transition in neutrophils, improved inflammation microenvironment of diabetic wounds, and contributed to wound regeneration. Our work is the first to utilize MNVs derived from inflammatory memory-activated EpSCs for tissue repair, in which the importance of neutrophil plasticity was also underscored. As the high-yield biomimetic nanovesicles, LEM present significant promising in diabetic wound treatment, which provide a novel alternative for tissue repair.

## Methods

### Cell culture and reagents

The EpSCs were sourced from the Institute of Basic Medical Science (IBMS) of CAMS & PUMC, which were isolated from skin sample and cultured in EpiLife (Gibco) medium supplemented with human keratinocyte growth supplement (HKGS; Gibco) at 37 °C in a 5% CO<sub>2</sub> environment. To characterize EpSCs, we performed immunofluorescence assays targeting cytokeratins K5 and K14, which serve as distinctive indicators of EpSCs. The presence of K5 and K14 within the EpSCs is clearly illustrated in Fig. S1A. Moreover, upon exposure to a high-calcium environment (1.5 mM CaCl<sub>2</sub>), these K5<sup>+</sup> and K14<sup>+</sup> cells were observed to express involucrin and loricrin—hallmarks of the final stages of epidermal cell maturation—as shown in Fig. S1B. This observation underscores the capacity of EpSCs to undergo epidermal differentiation. Primary neutrophils were isolated from C57BL/6 N mice by isolating the femur and tibia. The bones were then flushed with HBSS containing 0.38% sodium citrate buffer using a 25-gauge needle. The resulting cell suspension was passed through a 40 μm Corning cell strainer to achieve a uniform single-cell suspension. Red blood cells were lysed using Service bio's (Wuhan, China) red blood cell lysis buffer, employing a hypotonic lysis method. Neutrophils were then purified using Milteyni Biotec's magnetic-activated cell sorting (MACS) protocol, washed in HBSS, and cultured in RPMI-1640 at 37 °C with 5% CO<sub>2</sub>.

### LPS preconditioning protocols and CM collection

EpSCs were cultured until they reached 70% confluence, then treated either with PBS (EpSCs group) or 10 µg/ml LPS for 24 h (L-EpSCs group). To prepare the conditioned medium (CM), EpSCs were first rinsed with Dulbecco's Phosphate-Buffered Saline (DPBS) devoid of calcium and magnesium to remove any trace minerals that might affect the cells. Following the rinse, the cells were incubated for an additional 48 h to allow for the accumulation of secreted factors in the culture medium. After this incubation period, the supernatant was carefully collected to obtain the CM. The collected CM was then centrifuged at 1500 rpm for 10 min and filtered through a 0.22 µm membrane to pellet any remaining cells and debris. The filtered CM was subsequently subjected to ultrafiltration at 3000 g to concentrate the secreted factors. The resulting concentrated CM was then stored at -20 °C and used for subsequent in vivo experiments.

### miRNA/siRNA transfection

Small interfering RNAs (TLR4 siRNAs), miR-193a-5p mimics, miR-193a-5p inhibitors, and their respective control oligonucleotides were obtained from GenePharma. Transfections were conducted using Lipofectamine 2000 reagent (Invitrogen) following the manufacturer's instructions. The oligonucleotide sequences for TLR4 siRNAs are detailed in Table S1. Cells were subsequently collected for further analysis.

### Lentivirus vector constructs and transfection

Lentiviral vectors containing miR-193a-5p mimic (miR-193a<sup>OE</sup>), miR-193a-5p inhibitor (miR-193a<sup>KD</sup>), and their respective controls were purchased from GenePharma.

### Isolation and identification of EpSCs derived MNVs (EM)

EpSCs were divided into groups and treated with various substances: (1) PBS, (2) LPS (10 µg/ml), (3) LPS (10 µg/ml) combined with miR-193a<sup>OE</sup> (20µM), (4) LPS (10 µg/ml) combined with miR-NC<sup>OE</sup> (20µM), (5) LPS (10 µg/ml) combined with miR-193a<sup>KD</sup> (20µM), (6) LPS (10 µg/ml) combined with miR-NC<sup>KD</sup> (20µM). This resulted in the corresponding MNVs: (1) EM, (2) LEM, (3) miR-193a<sup>OE</sup>-LEM, (4) miR-NC<sup>OE</sup>-LEM, (5) miR-193a<sup>KD</sup>-LEM, (6) miR-NC<sup>KD</sup>-LEM. EpSCs were exposed to LPS in serum-free medium for 24 h before being returned to complete medium for further incubation. Upon reaching 80-90% confluence, EpSCs were washed twice with PBS. The cell pellets were reconstituted in PBS, and the suspension was extruded three times through 10 µm, 5 µm, and 1 µm polycarbonate membrane filters (Whatman, United States) using a mini-extruder (Morgtec, Shanghai, China) to obtain nanovesicles. The compacted nanovesicle suspension was filtered through a 0.22 µm filter and

subjected to ultracentrifugation at 100,000 g for 70 min, repeated twice at 4 °C, and stored at -80 °C for future use.

The size distribution of the nanovesicle was assessed using Nanoparticle Tracking Analysis (NTA). Their morphology was evaluated via transmission electron microscopy (TEM), and western blotting was used to probe for surface markers CD63, CD81, and TSG101.

### EM labeling and cellular uptake

EM were labeled with PKH67 green or PKH26 red fluorescent dyes following the Solarbio (China) protocol. This involved incubating EM with PKH67 or PKH26 and Diluent C for 5 min, terminating the reaction with 1% FBS, and then removing excess dye by ultrafiltration at 4000 g for 30 min. For in vivo studies, labeled EM were injected subdermally into mice, and tissues were collected at different time points, stained with DAPI, and examined by confocal microscopy. In vitro, mouse primary neutrophils were co-cultured with labeled EM, stained with Hoechst 33,258, and visualized with an inverted fluorescence microscope.

### Model for diabetic wounds and its treatment

Eight-week-old C56BL/6 N diabetic mice (db/db, SPF Biotechnology Co., Ltd; Beijing, China) were used for skin wound experiments according to international regulations outlined in the Guide for the Care and Use of Laboratory Animals. Animal procedures were approved by the Institutional Animal Ethics Committee. The wound site was prepared with an electric trimmer and 70% ethanol, then injured with an 8 mm biopsy punch. Wound healing progress was documented with photographs every other day. The wound treatments included applications of PBS, EM, LEM, miR-193a<sup>OE</sup>-LEM, miR-NC<sup>OE</sup>-LEM, miR-193a<sup>KD</sup>-LEM, or miR-NC<sup>KD</sup>-LEM. Before administration, the MNVs in EM and LEM were concentrated to a density of  $5.5 \times 10^8$  per 100 µL via ultrafiltration. These treatments were administered every other day at four distinct sites around the wound, with 100 µL (25 µL per site) being applied.

### Histological analysis

The injured tissues were treated with 4% paraformaldehyde, followed by a gradual dehydration process and embedding in paraffin. The tissues were then sliced into sections with 5 µm in thickness, and the hematoxylin and eosin (H&E) staining was conducted according to the H&E kit from Solarbio in China. The wound width and neoepithelium percentage were measured as described previously [27].

### Immunofluorescence

4% paraformaldehyde-fixed, paraffin-embedded tissue sections underwent de-waxing, rehydration, and antigen retrieval. To block endogenous peroxidase activity, the sections were treated with 3% H<sub>2</sub>O<sub>2</sub>, followed by blocking with 3% BSA for 1 h. The sections were then incubated with anti-mouse antibodies targeting Arg-1 (Proteintech, 1:400) and Ly-6G (ThermoFisher, 1:1000) for 12 h at 4 °C. Secondary antibodies were applied for 1 h at room temperature, followed by DAPI staining for nuclei. The results were captured using an inverted fluorescence microscope and analyzed with ImageJ software.

### Flow cytometry and gating strategy

Cell suspensions from skin samples ( $n = 3$ ) were washed with PBS and permeabilized using the eBioscience™ Foxp3/Transcription Factor Staining Buffer Set for flow cytometry, following the manufacturer's guidelines (00-5523-00). Conjugated antibodies were added and incubated for 1 h at room temperature. The antibodies included Alexa Fluor™ 700-CD11b (eBioscience, 56-0112-80, 1:100), FITC-Ly-6G (eBioscience, 11-5931-82, 1:400), and APC-Arg-1 (eBioscience, 17-3697-80, 1:100). Fluorescence data were collected using a flow cytometry, analyzed with FlowJo software, and validated using appropriate control antibodies. Gating strategy involved an initial selection for forward scatter (FSC) and side scatter (SSC) to isolate single live cells. This was followed by the positive selection of CD11b+ cells to enrich for myeloid cells. Within this enriched population, we identified Ly-6G+ cells to specifically target neutrophils. The expression of Arg-1 within the Ly-6G+ neutrophil subset was then evaluated to ascertain the fraction of cells displaying an anti-inflammatory phenotype.

### Neutrophil isolation by magnetic bead separation

Neutrophils were isolated from the skin wound site using a magnetic bead separation technique. Briefly, wound tissue was minced and digested with collagenase and DNase to obtain a single-cell suspension. The cells were then incubated with anti-Ly-6G magnetic microbeads (Miltenyi Biotec, Germany). After incubation, the cell suspension was passed through a magnetic column to selectively capture Ly-6G+ neutrophils. The unbound cells were removed by washing, and the neutrophils were eluted and collected for further analysis.

### Western blot analysis

Protein levels in samples were measured using the bicinchoninic acid (BCA) protein assay before being separated by SDS-PAGE. The proteins were then transferred to PVDF membranes, blocked with 5% BSA, and incubated with primary antibodies at 4 °C. This was followed by treatment with HRP-conjugated secondary

antibodies for 1 h at room temperature. Primary antibodies included CD63 antibody (1:1000, Beyotime, catalog no. AF1471), CD81 antibody (1:500, Beyotime, catalog no. AG1530), TSG101 antibody (1:500, Beyotime, catalog no. AF8259), TLR4 antibody (1:500, Beyotime, catalog no. AF8187), P38 antibody (1:500, Beyotime, catalog no. AF1111), phospho-P38 antibody (1:500, Beyotime, catalog no. AF5884), JNK antibody (1:500, Beyotime, catalog no. AF1048), phospho-JNK antibody (1:500, Beyotime, catalog no. AF1762),  $\beta$ -Actin antibody (1:50000, Abclonal, catalog no. AC038). Detection was carried out using the LAS-3000 Luminescent Image Analyzer.

### Quantitative reverse transcription PCR

RNA extraction was performed using the RNA Easy Fast Tissue/Cell Kit (TIANGEN, DP451). Cell-free total RNA concentration was measured with NanoDrop 2000. Reverse transcription was conducted using the ReverTra Ace qPCR RT Master Mix with gDNA remover (FSQ-301; Toyobo) kit and the miRNA RT Reagent kit (Accurate Biology, China). Quantitative reverse transcription PCR (qRT-PCR) was performed using the SYBR Green Kit from Vazyme (Nanjing, China). Primer sequences are listed in Table S2.

### Enzyme-linked immunosorbent assay (ELISA)

The cell culture supernatants were collected and stored at -20 °C for subsequent ELISA testing. The concentrations of various cytokines and proteins, including IL-1, IL-6, IL-12, TNF-alpha, IFN-gamma, HMGB1, IL-4, IL-10, IL-13, and TGF-beta, were quantified using specific ELISA kits. The experiment was conducted in strict accordance with the manufacturer's instructions. Initially, the cell culture supernatants were thawed and allowed to reach room temperature. Each well of a 96-well microplate was loaded with an appropriate volume of the supernatant. A primary antibody specific to the target cytokine or protein was then introduced into each well to allow binding with the antigen present in the samples. Following the primary antibody incubation, an enzyme-labeled secondary antibody was added to each well. This step facilitated the formation of an antibody-antigen-enzyme complex. The plates were then incubated for a specified period to allow for the development of the complex. After the incubation, a substrate solution was added to each well to initiate the enzyme-catalyzed color reaction. The reaction was allowed to proceed for a defined time, after which the absorbance was measured using a spectrophotometer (Leica Microsystems, Germany) at a wavelength specific for the colored product. The absorbance values were then used to calculate the concentration of each cytokine or protein in the samples according to the standard curve provided with the ELISA kits.

### Dual-luciferase reporter assay

The interaction between miRNAs and target genes was examined using a dual-luciferase reporter assay, as previously described [28]. Briefly, PsiCHECK2 vector from IGE Biotech (China), containing both the firefly luciferase gene (hLuc+) and the renilla luciferase gene (hRluc), was used. To investigate if miR-193a-5p directly targets TLR4, luciferase reporter plasmids with TLR4-wild-type (WT) and TLR4-mutant (MUT) sequences were synthesized. The TLR4 3' UTR sequence was inserted into PsiCHECK2-WT-TLR4 and PsiCHECK2-MUT-TLR4 vectors. These engineered plasmids were co-transfected into 293T cells along with miR-193a-5p mimics or miR-NC mimics using Lipofectamine® 3000 (Invitrogen; Thermo Fisher Scientific, Inc.). Post-transfection, luciferase activity was measured using Centro LB960 XS3 (Berthold, Germany).

### JC1 staining

$1 \times 10^6$  neutrophils were treated with PBS, EM, LEM (MNVs at a concentration of  $5.5 \times 10^8$ /ml) for 12 h and subsequently stained with JC1 from Solarbio (China) for 20 min at 37 °C. Fluorescent signals were observed and recorded using a fluorescent inverted microscope.

### ATP quantification

ATP levels in  $1 \times 10^6$  neutrophils treated with PBS, EM, LEM (MNVs at a concentration of  $5.5 \times 10^8$ /ml) for 12 h were measured using the ATP Assay Kit-Luminescence and the Glycolysis/OXPHOS Assay Kit (Dojindo, Japan).

### Fatty acid uptake

Fatty acid uptake in  $1 \times 10^6$  neutrophils treated with PBS, EM, LEM (MNVs at a concentration of  $5.5 \times 10^8$ /ml) for 12 h was assessed using the Fatty Acid Uptake Assay Kit (Dojindo, Japan). Fluorescent signals were visualized and captured with a fluorescent inverted microscope.

### Statistical analysis

All statistical analyses were performed using GraphPad Prism 8 InStat Software (San Diego, CA, USA). Data were presented as the mean  $\pm$  standard error of the mean (SEM) from at least three independent experiments. Group comparisons were made using the Student's t-test or ANOVA, with a p-value of less than 0.05 considered statistically significant. Statistical significance was indicated as \* $p < 0.05$ , \*\* $p < 0.01$ , \*\*\* $p < 0.001$ .

## Results and discussion

### Inflammatory memory activated-EpSCs accelerated diabetic wound healing and mitigated excessive inflammatory response

In order to assess if an inflammatory trigger could activate the paracrine activity of EpSCs [13, 14, 16, 17], we exposed EpSCs to LPS (L-EpSCs) (Fig. 1A) and examined the alterations in the cytokines they secreted. ELISA testing indicated that EpSCs under inflammation pressure secreted higher levels of anti-inflammatory cytokines and pro-healing factors including IL-4, IL-13, and TGF- $\beta$  (Fig. 1B) [29, 30]. These findings suggested that inflammatory memory activated-EpSCs may have the potential to mitigate the excessive inflammatory response in the process of wound healing, particularly in diabetic wounds. Further, we evaluated the impact of conditioned media (CM) obtained from EpSCs (EpSCs-CM) or L-EpSCs (L-EpSCs-CM) on tissue regeneration in diabetic mice with excisional cutaneous wounds. Compared with PBS control or EpSCs-CM treated wounds, topical administration of L-EpSCs-CM on skin wounds resulted in faster wound healing (Fig. 1C). Wound areas were time-dependently decreased in all experimental conditions, with the most noticeable decrease occurring on day 5 or 7 in L-EpSCs-CM treated group (Fig. 1D). Additional research was carried out on the chemokine and cytokine profile specific to tissues that affect the recruitment and polarization of neutrophils [5]. Administration of L-EpSCs-CM was found to significantly reduce the levels of CCL2, CCL3, and CCL5, crucial for neutrophil recruitment, when compared to control or EpSCs-CM treated wounds (Fig. 1E). At the same time, the levels of IL-4 and IL-13 in L-EpSCs-CM groups were increased, which are important for acquiring N2 neutrophil phenotype, and meanwhile, the levels of IFN-gamma, a key cytokine for N1 neutrophil differentiation, were reduced in L-EpSCs-CM groups (Fig. 1F). To understand the effect of EpSCs and L-EpSCs on neutrophils, we co-cultured neutrophils with EpSCs or L-EpSCs and validated whether this cell-cell interaction could switch neutrophils to N2 anti-inflammatory phenotype (Fig. 1G). The mRNA expression profiles by qRT-PCR revealed the significant increases of N2 neutrophil markers including CD163, CD206 and Arg-1 in the co-culture system of L-EpSCs and neutrophils, indicating the potential of inflammatory memory-activated EpSCs to manipulate neutrophil plasticity (Fig. 1H). These findings suggested that inflammatory stress could enhance the repair ability of EpSCs in diabetic wound, and the activated EpSCs have the strong capability of driving the phenotypic transition of neutrophils into N2 anti-inflammatory subtype.

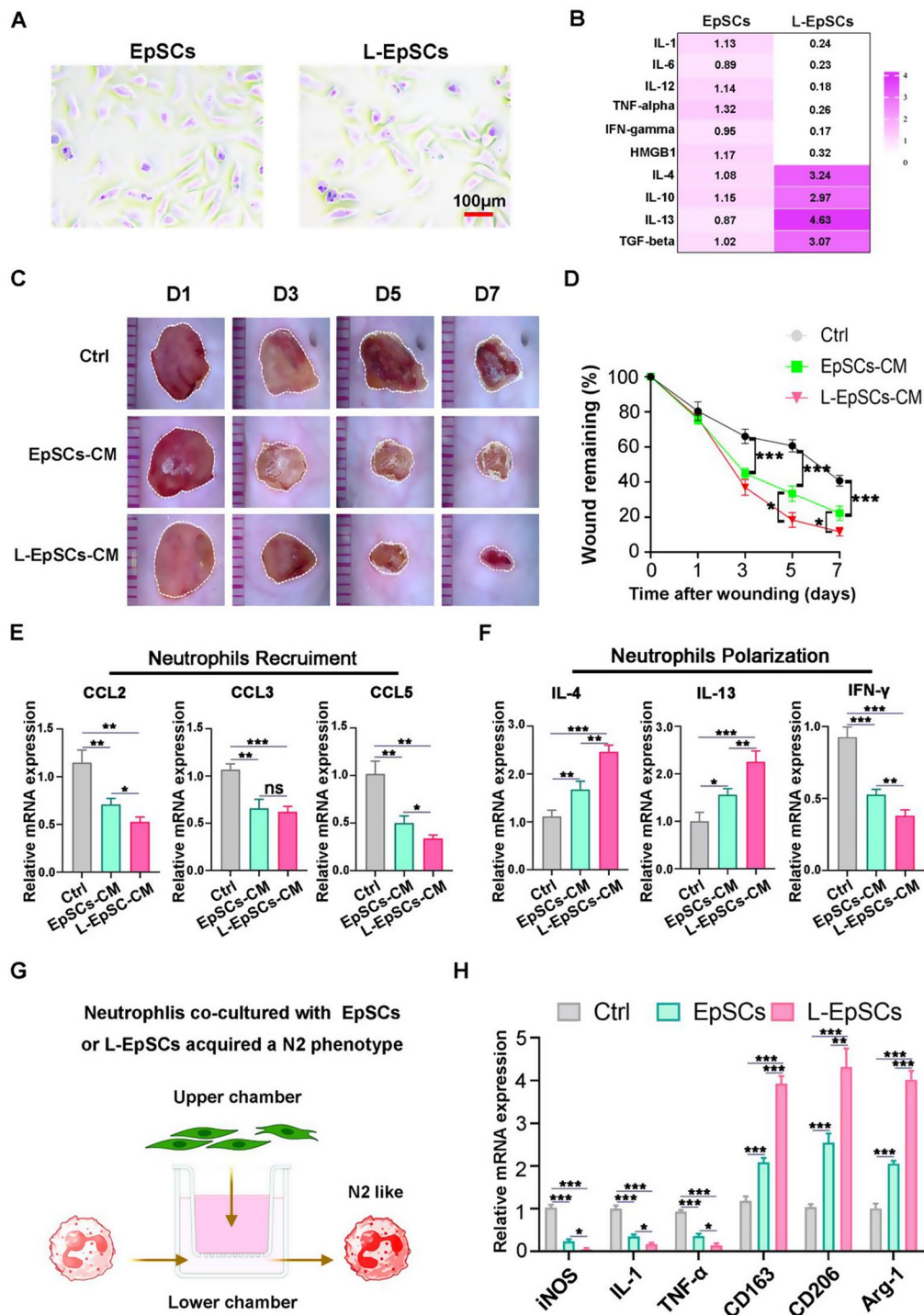


**Fig. 1** EpSCs under inflammatory pressure promoted diabetic wound healing and induced N2 polarization. **(A)** Morphological changes in EpSCs activated by LPS under light microscopy. Scale bar = 100 nm. **(B)** Heat map showing the relative expression patterns of pro-inflammatory and anti-inflammatory cytokines in naïve and active EpSCs, as determined by ELISA. The color intensity represents the expression levels, with darker shades indicating higher concentrations. **(C)** The gross view of wounds in the control group, EpSCs-CM group, and L-EpSCs-CM group was observed on days 1, 3, 5, and 7. **(D)** Measuring the extent of wound healing in **(C)**.  $n=3$  per group. **(E)** qRT-PCR analyzed the levels of chemokines CCL2, CCL3, and CCL5. A sample size of three was used in each group for the experiments, with GAPDH serving as an internal control for normalization. **(F)** Cytokines IL-4, IL-13, and IFN-gamma were analyzed using qRT-PCR for their expression levels. A sample size of three was used in each group for the experiments, with GAPDH serving as an internal control for normalization. **(G)** Schematic illustration of the experimental process depicting the co-cultivation of EpSCs and neutrophils. **(H)** Quantitative PCR is used to measure the gene expression of N1 markers (iNOS, IL-1, TNF- $\alpha$ ) and N2 markers (Arg-1, CD163, CD206) in neutrophils that are co-cultured with EpSCs or L-EpSCs. Data represents the mean  $\pm$  SEM from three separate experiments. ns indicated no significant difference; \* $P < 0.05$ ; \*\* $P < 0.01$ ; \*\*\* $P < 0.001$ .

### Construction and characterization of MNVs derived from inflammatory memory activated-EpSCs

The favorable regenerative effect of L-EpSCs inspired us to develop nanovesicles with promising clinical prospect. Although EVs and MNVs are both promising nanovesicles in the field of tissue regeneration, the amount of cells required in the preparation process of EVs is too large, in contrast to MNVs, which can be obtained directly by gradient mechanical extrusion of cells, with a high degree of efficiency [23]. To obtain a pool of EpSCs-MNV (EM) and LPS-EpSCs-MNV (LEM), EpSCs and L-EpSCs were collected and passed through multiple polycarbonate membranes with varying pore sizes (Fig. S2A). Following this, the centrifuge was used to concentrate MNVs and remove small molecules, finally producing EM and LEM with an average size of 135.6 nm and 139.3 nm, respectively (Fig. S2B). NTA unveiled a concentration of approximately  $5.5 \times 10^8$ /ml for these MNVs (Fig. S2B). Transmission electron microscopy (TEM) images revealed that the composition of EM and LEM closely resembled exosomes, displaying a circular cup-like shape surrounded by lipid membranes (Fig. S2C). The exosomes markers including CD63 and CD81, detected by Western blotting (Fig. S2D), provided additional evidences supporting the similarities between EVs and MNVs. To further elucidate the uptake of EM and LEM in the skin, we used fluorescence microscopy to examine the presence of EM and LEM. Four hours post-treatment, a significant build-up of PKH67-labeled EM and LEM could be seen surrounding the perinuclear regions of skin cells (Fig. S2E), which indicated that skin cells can absorb EM and LEM internally.

### Effect of LEM on diabetic wound healing and neutrophil reprogramming

In order to study the pro-healing capabilities of LEM in vivo, full-thickness excisional wounds were created on the skin back in diabetic models, pictures were taken of the wounds, and the changes in wound size were documented to visually display the process of healing. On postoperative day (POD) 0, the EM or LEM were administered intradermally near the wound border. The progress of the healing wounds was documented for additional analysis on POD 1, 3, 5, and 7. The rapid healing of wounds in the LEM groups was noticed on POD 5, and became even more pronounced on POD 7 (Fig. 2A). By POD 7, the average wound size in LEM-treated mice had significantly decreased to  $7.18 \pm 2.16$  mm<sup>2</sup>. To express the wound healing progress, we calculated the average remaining wound area rate (actual wound area/initial wound area), which was 8.69% for the LEM-treated group (Fig. 2B). In contrast, the control and EM treatment groups had average remaining area rates of 38.94% and 17.86%, respectively, on POD 7 (Fig. 2B). The schematic

diagram in Fig. 2A depicted the dynamic healing process of each group at various time points for visualization purposes. In order to further evaluate the in vivo efficacy of LEM in promoting wound healing, the regenerated skin wounds were subjected to H&E staining on POD 7 for further analysis (Fig. 2C). The wound specimens were evaluated according to the method described [27]. Analysis of the newly formed epidermis over the wound demonstrated that treatment with LEM not only accelerated newly formed epithelium (NFE), but also led to a notable expansion in hyperproliferative epidermis (HPE) (Fig. 2D and E). Similarly, a reduction in wound size (Fig. 2F) and a notable increase in wound closure rate (Fig. 2G) were observed in LEM-treated mice, indicating a beneficial impact of LEM on facilitating quick re-epithelialization and enhancing skin wound regeneration in vivo. Building on prior research, we delved deeper into the unique chemokine and cytokine patterns in tissues that impact the recruitment and polarization of neutrophils. The findings indicated that wounds topically treated with LEM exhibited decreased levels of CCL2, CCL3, CCL5, and IFN-gamma, while significantly increased levels of IL-4 and IL-13 (Fig. 2H and I). With the aim of clarifying the effect of LEM on neutrophil recruitment and polarization, we employed flow cytometry for further quantitative analysis. The results showed that the quantity of infiltrating neutrophils in the wound site was similar across all groups on POD 1 and 3. Nevertheless, the number of neutrophils in the EM and LEM group started to decline on POD 5 and 7, whereas it remained elevated in the control group (Fig. S3). We additionally confirmed the percentage of N2 subtype among all neutrophils. During the first 7 days of wound healing, we observed a gradual rise in the percentage of N2 subtype neutrophils in wounds treated with LEM, peaking at 75.81% on POD 7. However, their proportions in control and EM treated wounds were 8.23% and 48.62%, respectively (Fig. 2J and K). Taken together, these findings emphasized the beneficial impact of LEM on promoting skin repair and controlling an overactive inflammatory response in diabetic wounds.

### LEM initiated mitochondrial metabolic reprogramming to induce N2 anti-inflammatory phenotype in neutrophils

N2 neutrophils, due to their substantial energy needs, are dependant on the mechanisms of elevated oxidative phosphorylation (OXPHOS) and lipid oxidation. The enhanced activity of fatty acid uptake and fatty acid oxidation (FAO) serve as a primary energy source to meet the metabolic requirements for N2 polarization [5]. In an attempt to determine if LEM trigger metabolic reprogramming in neutrophils, we exposed neutrophils to EM and LEM and observed metabolic alterations (Fig. 3A). During coculture, EM and LEM could be intake easily by

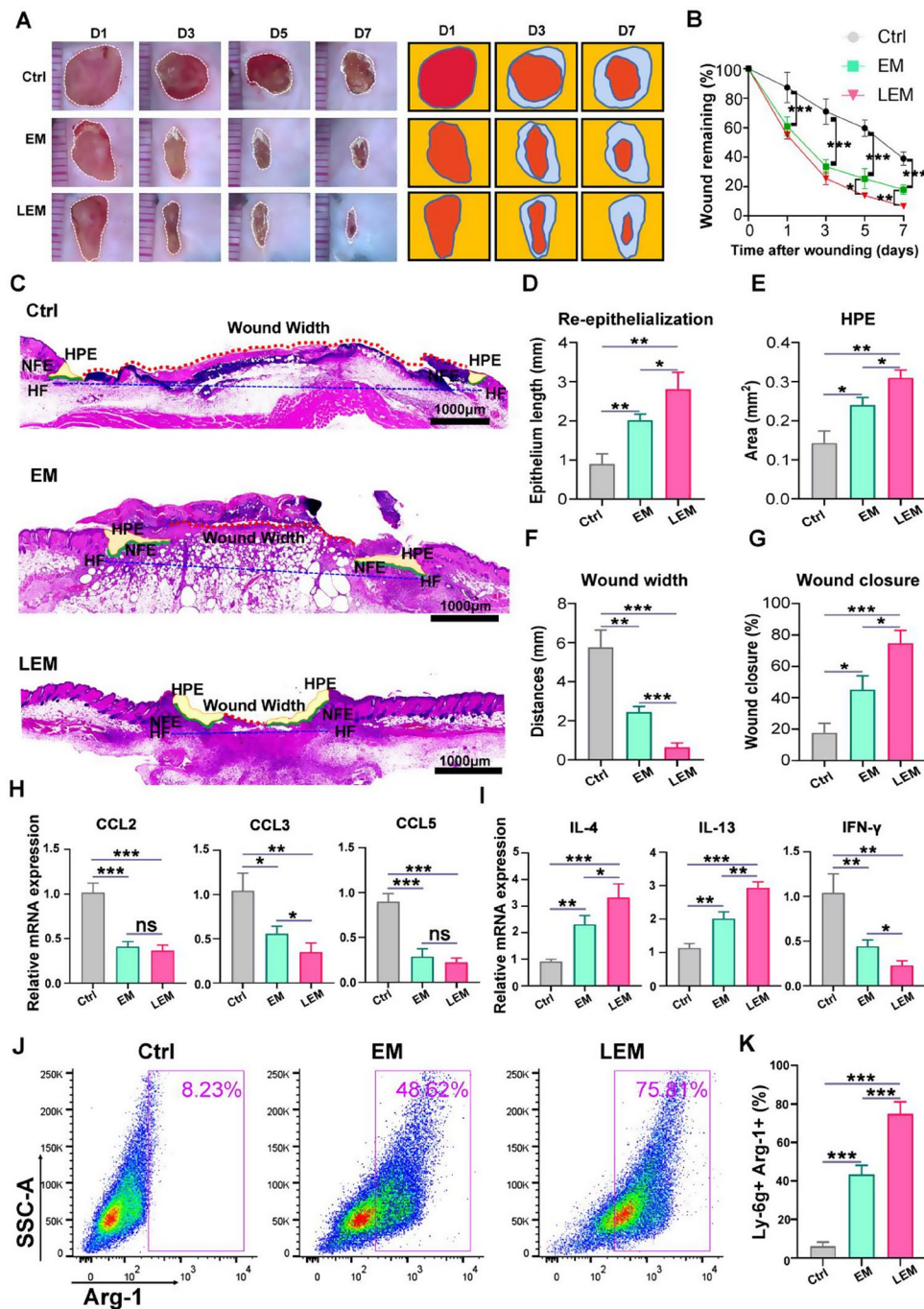


**Fig. 2** EpSCs under inflammatory pressure promoted diabetic wound healing and induced N2 polarization. **(A)** The overall observation of injuries in the control group, EM group, and LEM group was conducted on days 1, 3, 5, and 7. **(B)** Measuring the extent of wound healing in **(A)**.  $n=3$  per group. **(C)** Hematoxylin and eosin (H&E) stained sections of untreated and wounds treated with EM or LEM on day 7 were analyzed for the length of newly formed epithelium (NFE, Green line), area of hyperproliferative epidermis (HPE), wound width (Red dotted line), percentage of wound closure (NFE/NFE + wound width  $\times$  100%), and wound contraction (distance between wound border hair follicles (HF), blue dotted line). This analysis was conducted as described previously. **(D-G)** Statistics of wound sections for **(D)** re-epithelialization, **(E)** area of HPE, **(F)** wound width and **(G)** wound closure in control, EM or LEM treated mice ( $n=3$ ). **(H)** qRT-PCR was used to analyze the levels of chemokines CCL2, CCL3, and CCL5. A sample size of three was used in each group for the experiments, with GAPDH serving as an internal control for normalization. **(I)** qRT-PCR was used to analyze the levels of IL-4, IL-13, and IFN-gamma cytokines. A sample size of three was used in each group for the experiments, with GAPDH serving as an internal control for normalization. **(J)** Flow cytometry was used to examine the percentage of N2 phenotype neutrophils (Ly-6G + Arg-1+) in diabetic wounds that were treated with PBS, EM, or LEM. **(K)** Quantitative evaluation of the findings in **(J)** with a sample size of 3. Data represents the mean  $\pm$  SEM from three separate experiments. ns indicated no significant difference;  $*P < 0.05$ ;  $**P < 0.01$ ;  $***P < 0.001$

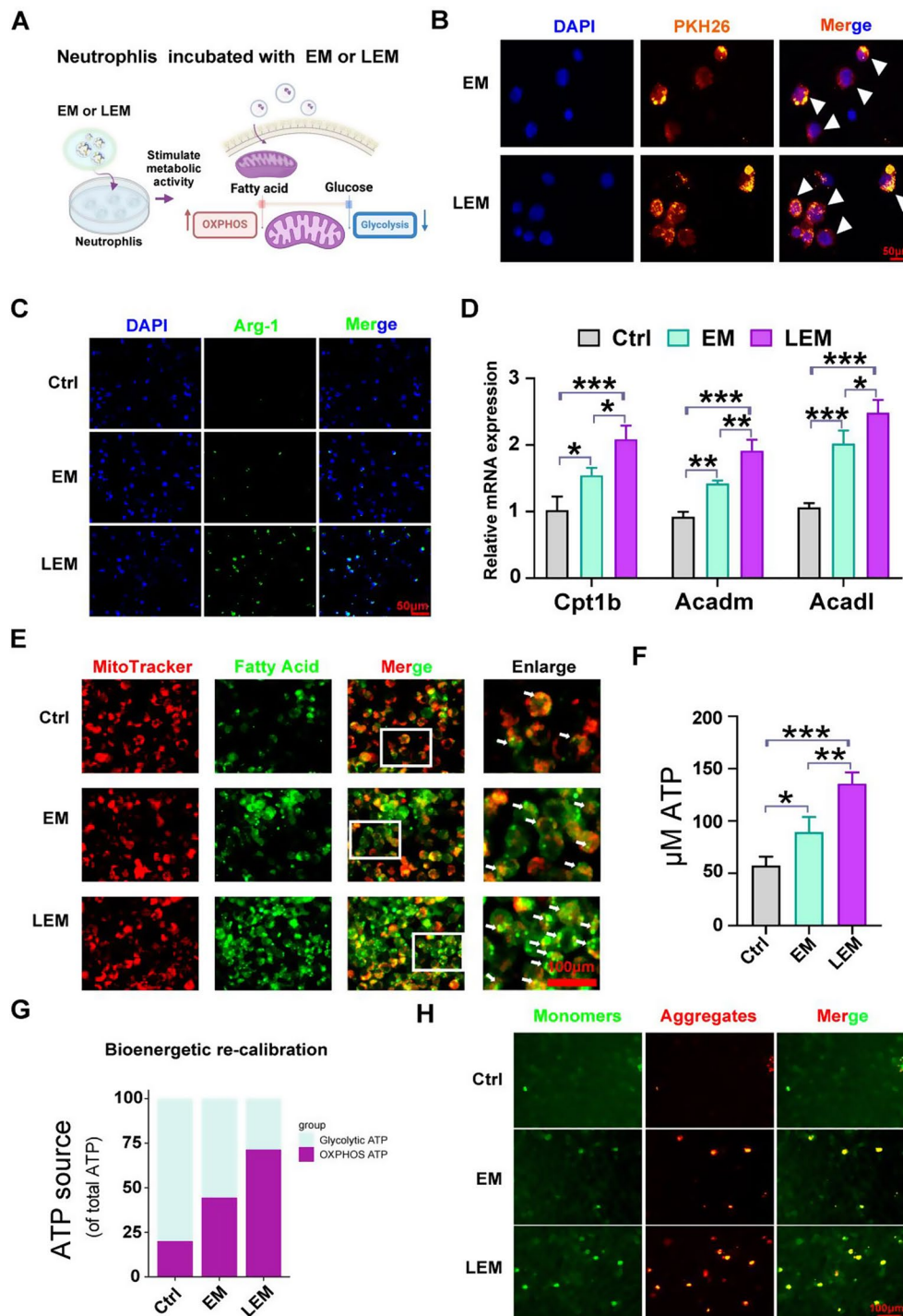


**Fig. 3** LEM promoted metabolic recalibration in neutrophil mitochondria and induced N2 polarization. **(A)** Schematic diagram of the experimental procedure showing EM and LEM activated mitochondrial metabolic activity in mouse primary neutrophils. **(B)** Fluorescent images showing PKH26-tagged EM, as well as LEM taken in by mouse primary neutrophils stained with DAPI; scale bar: 50 μm. **(C)** Changes in the expression of Arg-1 in N2 polarization by immunofluorescence. **(D)** Transcription levels of genes related to fatty acid oxidation (*Cpt1b*, *Acadm*, and *Acadl*) were measured in mouse primary neutrophils following treatment with EM and LEM. **(E)** Fatty acid uptake of mitochondria was examined in mouse primary neutrophils following treatment with EM and LEM. Scale bars, 100 μm. **(F)** Mouse primary neutrophils' cellular ATP levels. **(G)** ATP levels in oxidative phosphorylation and glycolysis in mouse primary neutrophils. **(H)** Representative pictures showing JC-1 staining in primary neutrophils from mice. JC-1 produces red fluorescent aggregates when mitochondrial potentials are high and retains green fluorescent monomers when mitochondrial potentials are low. Scale bars, 100 μm. Data represents the mean ± SEM from three separate experiments. ns indicated no significant difference; \*P < 0.05; \*\*P < 0.01; \*\*\*P < 0.001

neutrophils, as shown in Fig. 3B, PKH26-labeled EM and LEM are internalized by neutrophils and concentrated in the perinuclear area. After that, EM and LEM skewed neutrophils to an N2 phenotype, and as shown in immunofluorescence, EM and LEM primed neutrophils to express N2 marker Arg-1 (Fig. 3C). Notably, more neutrophils expressing Arg-1 were observed in LEM treatment group compared with the ones in EM treatment group (Fig. 3C).

Our prior studies indicated that lipid metabolism, specifically fatty acid oxidation (FAO), is crucial for N2 polarization [5]. In the present research, we found that LEM caused a surge in the expression of FAO genes (*Cpt1b*, *Acadm*, and *Acadl*) at the mRNA level, as shown in Fig. 3D. Furthermore, following treatment with LEM, neutrophil mitochondria enhanced its cellular uptake of fatty acid, as shown in Fig. 3E. This enhancement was also associated with changes in ATP generation [31]. The ATP quantitative analysis indicated that the increased FAO in L-MNVs-EpSCs treated neutrophils was associated with a notable rise in ATP levels, emphasizing a shift in energy metabolism (Fig. 3F). Our metabolic study supported the change in energy levels, showing notable alterations in OXPHOS and glycolysis caused by L-MNVs-EpSCs (Fig. 3G). Furthermore, the mitochondria in neutrophils treated with LEM displayed an elevated membrane potential, as indicated by a greater amount of red-Fluorescent aggregates from JC-1 staining, in contrast to the control or EM treated cells with low membrane potential in their mitochondria (Fig. 3H). These results suggested that LEM triggered mitochondrial metabolic recalibration in neutrophils, supplying more “fuel” for phenotypic switching to an anti-inflammatory subtype.

#### **LEM transferred miR-193a-5p to inhibit the TLR4/MAPK pathway in neutrophils**

Several research studies have verified the impact of miR-193a in inhibiting inflammation [32, 33]. A recent study has shown that miR-193a-5p could potentially regulate the balance between N1 and N2 phenotypes in neutrophils, reducing neuroinflammation-induced ischemic damage [34]. In psoriasis, miR-193a expression in EpSCs had been reported to regulate inflammatory process, and loss of miR-193a in EpSCs showed increased skin lesions and higher inflammation activity [35]. Our research also found an increased miR-193a-5p expression in L-EpSCs and LEM, as well as in neutrophils exposed to LEM (Fig. 4A-C). These results indicated that LEM can transport more miR-193a-5p into neutrophils.

In order to investigate how miR-193a-5p in LEM contribute to N2 polarization, we utilized miRWalk and miRBase database to predict the target genes of miR-193a-5p [36]. Based on the Venn diagram analysis, a total of 28 genes were identified through the utilization

of R software (Fig. 4D). TLR4 was identified as a potential target of miR-193a-5p through bioinformatic analysis and review of existing literature, as shown in Fig. 4E. To validate this hypothesis, a luciferase assay was utilized to detect the relationship between miR-193a-5p and TLR4. Luciferase reporter plasmids containing either wild-type (WT) or mutant (Mut) 3' UTR sequences of TLR4, with potential binding sites, were cloned and co-transfected with miR-193a-5p mimic or miR-NC mimic into 293T cells. The findings indicated that increased expression of miR-193a-5p greatly inhibited the luciferase reporter activity of the vector containing the wild-type binding site, while having no effect on the mutant binding site (Fig. 4F). Furthermore, qRT-PCR findings indicated that the mRNA levels of TLR4 in neutrophils were suppressed by the introduction of miR-193a-5p mimic, while miR-193a-5p inhibitor resulted in an increase expression of TLR4 (Fig. 4G and H). These results suggested that miR-193a-5p may partially involved in the biological functions of LEM. We further investigated whether EM or LEM could induce similar inhibition in neutrophils, and miR-193a-5p inhibitor was used. The findings indicated that a notable decrease in TLR4 mRNA levels in neutrophils treated with LEM, but this effect was reversed by adding miR-193a-5p inhibitor (Fig. 4I). In addition, Western blot analysis indicated that both EM and LEM significantly reduced TLR4 protein expression, with LEM being more effective. However, inhibition of miR-193a-5p impeded this response (Fig. 4J). These results suggest that miR-193a-5p targets the gene expression of TLR4.

There are growing evidences showing that the the activation of the mitogen-activated protein kinase (MAPK) pathway, which includes c-JUN N-terminal Kinase (JNK) and P38, may play the essential role in regulating immune cell plasticity [37–39]. Analysis of KEGG pathways indicated that miR-193a-5p may control the MAPK signaling pathway (Fig. 4K and L). Therefore, we conducted a more in-depth investigation to observe the levels of phosphorylated JNK (p-JNK) and phosphorylated P38 (p-P38) in neutrophils following exposure to EM and LEM. The findings suggested the notable decrease in the p-JNK level and p-P38 level both in EM-treated and LEM treated neutrophils, and lower levels of the p-JNK and p-P38 were observed in LEM-treated cells (Fig. 4M-O). Notably, this effect was dampened by miR-193a-5p inhibitor (Fig. 4M-O). These results suggested that LEM delivered miR-193a-5p into neutrophils and induced downregulation of TLR4-JNK/P38 MAPK signaling pathway, which may be responsible for LEM-induced switching on N2 polarization.

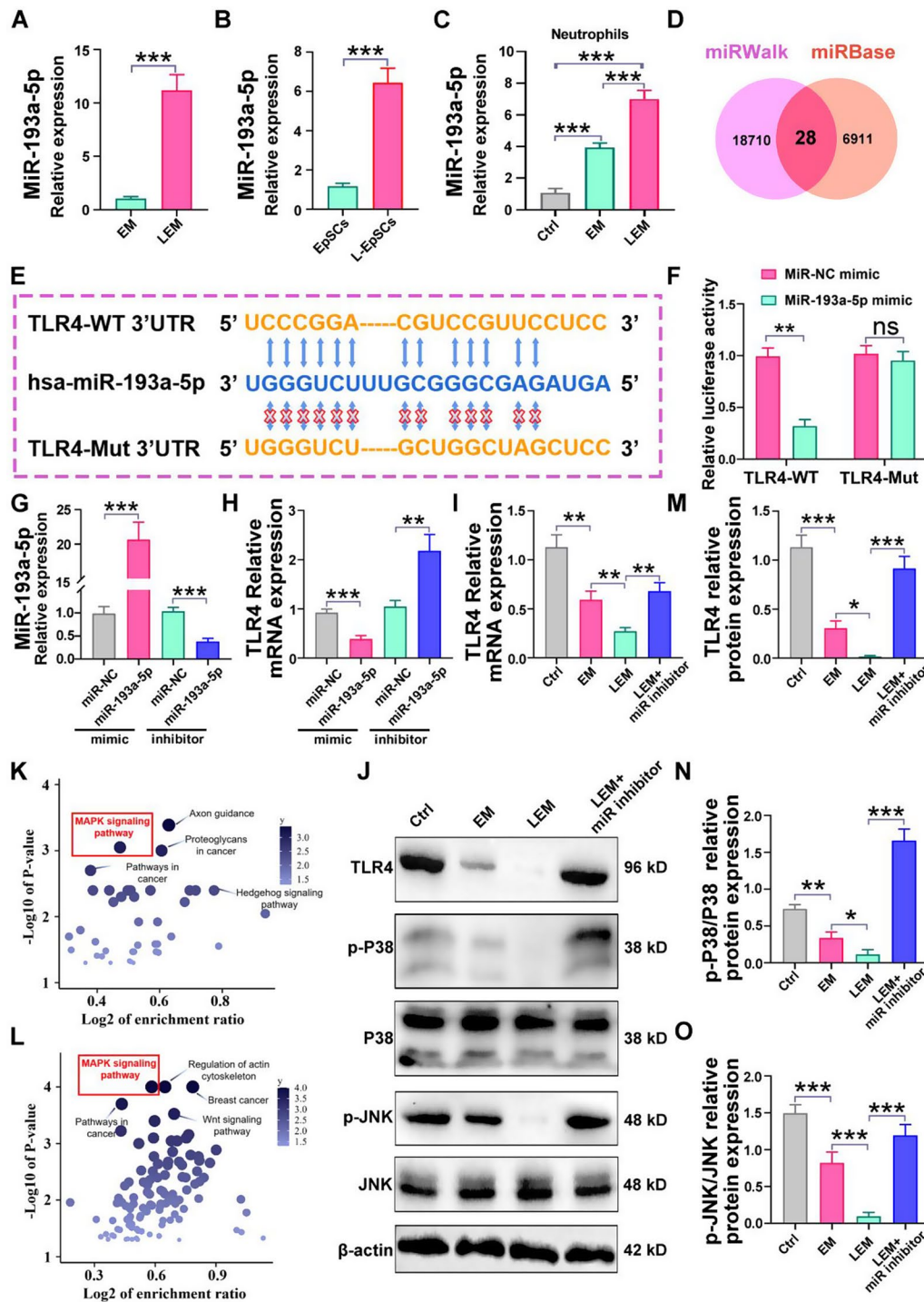


**Fig. 4** LEM transferring miR-193a-5p downregulated the TLR4/MAPK pathway in vitro. **(A)** qRT-PCR measured the expression level of miR-193a-5p in EpSCs and L-EpSCs. **(B)** qRT-PCR measured the expression level of miR-193a-5p in EM and LEM. **(C)** qRT-PCR measured the expression level of miR-193a-5p in neutrophils after exposure to engineered EM and LEM. **(D)** The potential target genes of miR-193a-5p were identified through miRWalk and miRBase database analysis. The Venn diagram revealed that R software identified 28 genes. **(E)** Anticipated interaction site of miR-193a-5p with TLR4. **(F)** Luciferase reporter assay confirmed the interaction of miR-193a-5p with TLR4. **(G)** miR-193a-5p expression in neutrophils was measured using qRT-PCR after transfection with either a miR-193a-5p mimic or inhibitor. **(H)** TLR4 mRNA levels in neutrophils were measured by qRT-PCR following transfection with either a miR-193a-5p mimic or inhibitor. **(I)** TLR4 mRNA levels were measured in neutrophils following treatment with EM, LEM, and LEM plus miR-193a-5p inhibitor using qRT-PCR. **(J)** TLR4 protein, P38, p-P38, JNK, and p-JNK expression levels in neutrophils were analyzed using Western blot after treating with EM, LEM, and LEM plus miR-193a-5p inhibitor. **(K-L)** Analysis of KEGG pathways revealed the participation of the MAPK signaling pathway downstream of miR-193a-5p. **(M-O)** Protein expression levels of TLR4, p-P38/P38, and p-JNK/JNK were quantified using Image J software. Data represents the mean  $\pm$  SEM from three separate experiments. ns indicated no significant difference; \* $P < 0.05$ , \*\* $P < 0.01$ ; \*\*\* $P < 0.001$

### LEM skewed N2 neutrophil polarization through manipulating miR-193a-5p/TLR4/JNK/P38 MAPK pathways

Lentiviral infection was utilized to establish miR-193a-5p overexpression (miR-193a<sup>OE</sup>) and knockdown (miR-193a<sup>KD</sup>) in L-EpSCs to investigate the direct impact of miR-193a-5p on N2 polarization, along with the respective negative controls (miR-NC<sup>OE</sup> and miR-NC<sup>KD</sup>). qRT-PCR confirmed the transfection efficiency in EpSCs (Fig. 5A). Subsequently, MNVs were isolated from these engineering L-EpSCs and designated as miR-193a<sup>OE</sup>-LEM, miR-NC<sup>OE</sup>-LEM, miR-193a<sup>KD</sup>-LEM, and miR-NC<sup>KD</sup>-LEM, according to their parent cells. Furthermore, the miR-193a-5p expression level was measured in these MNVs, showing a comparable pattern to that observed in EpSCs (Fig. 5B). Following administration of these MNVs, there was a notable increase in miR-193a-5p levels in the miR-193a<sup>OE</sup>-LEM-treated neutrophils compared to the miR-NC<sup>OE</sup>-LEM-treated cells. Conversely, the introduction of miR-193a<sup>KD</sup>-LEM led to a notable reduction of miR-193a-5p levels in neutrophils when compared to miR-NC<sup>KD</sup>-LEM (Fig. 5C). Significantly, treating neutrophils with miR-193a<sup>OE</sup>-LEM led to a decrease in TLR4 expression, while the neutrophils in miR-193a<sup>KD</sup>-LEM group showed the opposite outcome (Fig. 5D and E). Subsequently, the MAPK signaling pathway was also assessed in neutrophils following the introduction of these MNVs. Our observation showed that increased levels of miR-193a-5p led to a notable decrease in the levels of p-JNK and p-P38 (Fig. 5D, F and G). In contrast, the levels of p-JNK and p-P38 were higher in the miR-193a<sup>KD</sup>-LEM group compared to the miR-NC<sup>KD</sup>-LEM group (Fig. 5D, F and G). After incubating for 12 h, we analyzed the levels of N1 and N2-related markers in neutrophils using qRT-PCR. The findings showed that miR-193a<sup>OE</sup>-LEM treatment caused a notable change in neutrophils towards the N2 phenotype, with reduced expression of N1 markers (iNOS, IL-1, and TNF- $\alpha$ ) (Fig. S4A-C), but a high expression level of N2 markers (CD163, CD206, and Arg-1) (Fig. 5H-I, Fig. S4D-F). These findings suggest that miR-193a-5p in MNVs plays a crucial role in inhibiting TLR4/MAPK pathway and affecting neutrophil plasticity.

To further investigate the mechanism by which MNVs miR-193a-5p induces N2 polarization through targeting TLR4, we conducted a rescue experiment. We found that knockdown of TLR4 could partially reverse the regulatory effect of MNVs miR-193a-5p on the MAPK signaling pathway (Fig. S5A-E). Additionally, the expression of N1 markers induced by miR-193a<sup>KD</sup>-LEM was inhibited after TLR4 silencing (Fig. S5F-G), while the expression of N2 markers exhibited the opposite trend (Fig. S5I-K). These results indicated that MNVs miR-193a-5p can induce N2 polarization of neutrophils by downregulating the TLR4/JNK/P38 MAPK pathway.

### miR-193a-5p overexpression enhanced the repair ability of LEM and significantly facilitated diabetic wound regeneration

In order to more accurately ascertain the function of LEM miR-193a-5p in controlling N2 polarization in vivo, miR-193a<sup>OE</sup>-LEM, miR-NC<sup>OE</sup>-LEM, miR-193a<sup>KD</sup>-LEM, or miR-NC<sup>KD</sup>-LEM were administered intradermally near the edge of the diabetic wound every other day. The miR-193a<sup>OE</sup>-LEM treated mice showed a notable increase in wound healing speed compared to the control groups, as indicated by both macroscopic measurements and morphometric analysis (Fig. 6A and B). Additionally, a morphometric assessment was conducted on wound samples on POD 7 to assess the progression of wound healing at both the tissue and cellular levels (Fig. 6C). Analysis of the newly formed epidermis over the injury skin indicated that increased levels of miR-193a-5p in LEM not only led to quicker re-epithelialization (NFE) but also a notable expansion in regions of hyperproliferative epidermis (HPE) (Fig. S6A and B). Similarly, a reduction in wound size (Fig. S6C) and a notable enhancement in wound healing speed (Fig. S6D) were observed in mice treated with miR-193a<sup>OE</sup>-LEM, while miR-193a<sup>KD</sup>-LEM exhibited a contrasting pattern. In addition, the findings from the chemokine and cytokine profile in miR-193a<sup>OE</sup>-LEM-treated wounds revealed the reduced levels of CCL2, CCL3, and CCL5, as well as IFN-gamma, while notably increased levels of IL-4 and IL-13 in wound site (Fig. 6D-I). These results illustrated the beneficial effects of miR-193a-5p on enhancing the healing of skin wounds and improving the inflammatory dysregulation in vivo.

Since LEM induced neutrophil polarization to N2 phenotype (as depicted in Fig. 2J), we investigated if upregulation of miR-193a-5p in LEM improved the functionality of LEM. Flow cytometry was used to measure the N2 phenotype proportion of neutrophils in wounds, revealing that the overexpression of miR-193a-5p in LEM primed more neutrophils to the N2 phenotype compared to naïve LEM (Fig. 7A and B). Of note, at POD 7, the proportion of N2 neutrophils in miR-193a<sup>OE</sup>-LEM treated wounds surged significantly to  $91.18 \pm 4.17\%$ , compared to the naïve LEM treated wounds of  $74.80 \pm 4.63\%$ . Expectedly, knockdown of miR-193a-5p in LEM led to an opposite trend, in which the proportion of N2 neutrophils was  $37.18 \pm 4.63\%$ , compared to  $71.53 \pm 5.72\%$  of corresponding negative controls (Fig. 7B). We further validated this results by tissue immunofluorescence on wound sections. Immunofluorescence staining revealed increased N2 marker Arg-1 expression in neutrophils (labeled Ly-6G) at the wound site, indicating a higher number of neutrophils transitioning to the N2 phenotype in wounds treated with miR-193a<sup>OE</sup>-LEM compared to the miR-NC<sup>OE</sup>-LEM group on POD 7. Conversely, administering miR-193a<sup>KD</sup>-LEM resulted in a lower

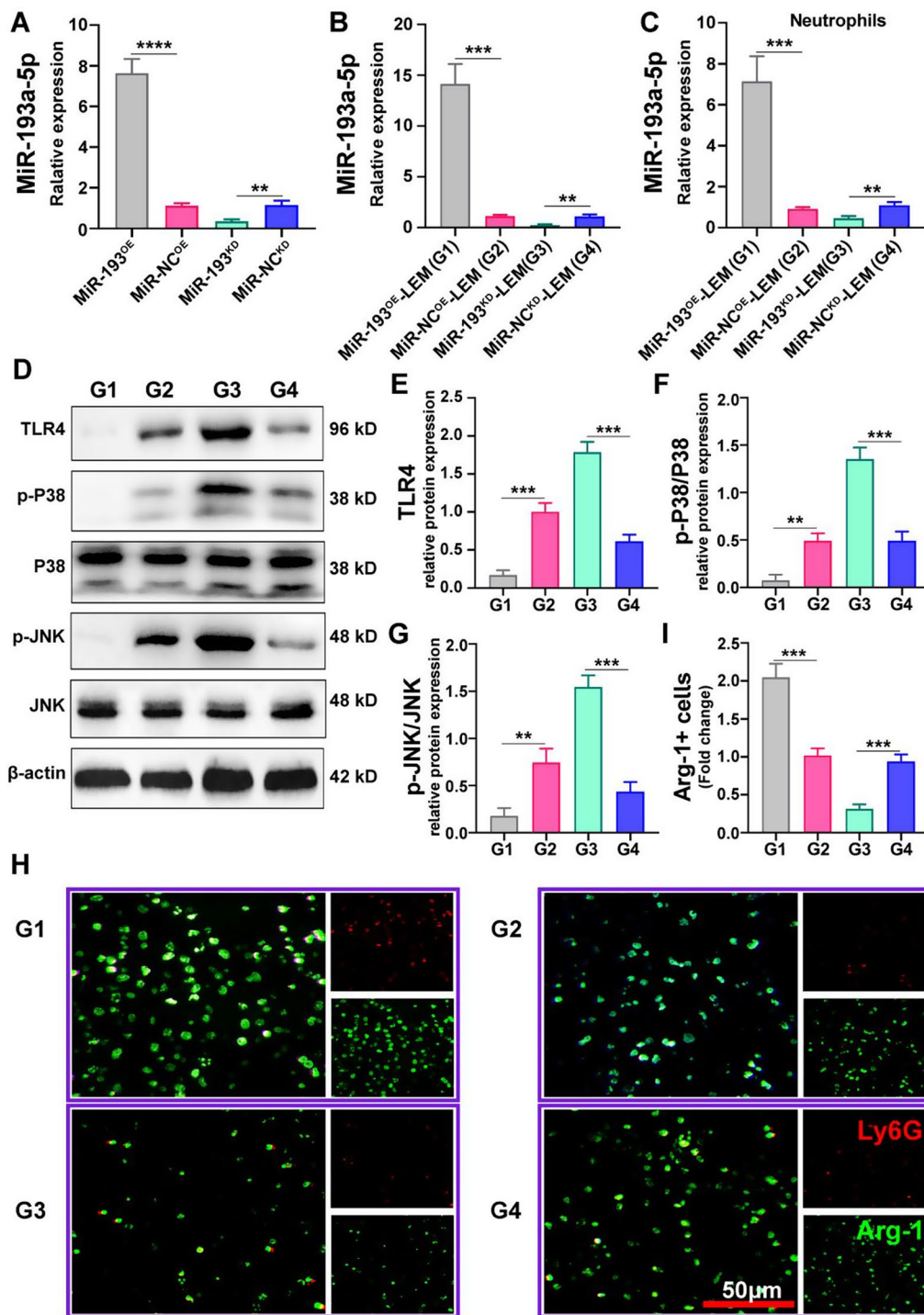


**Fig. 5** The upregulation of miR-193a-5p in LEM inhibited the TLR4/Mapk pathway and promoted N2 polarization. **(A)** qRT-PCR measured the expression level of miR-193a-5p in EpSCs that were either overexpressing miR-193a-5p (miR-193a<sup>OE</sup>), knocking down miR-193a-5p (miR-193a<sup>KD</sup>), or in the respective negative control groups. **(B)** The miR-193a-5p expression levels were assessed using qRT-PCR in miR-193a-5p overexpressed and knockdown LEM, as well as its control groups. **(C)** miR-193a-5p expression levels were assessed in neutrophils following exposure to miR-193a<sup>OE</sup>-LEM, miR-NC<sup>OE</sup>-LEM, miR-193a<sup>KD</sup>-LEM, and miR-NC<sup>KD</sup>-LEM using qRT-PCR. **(D)** Western blot was performed to analyze the expression levels of TLR4 protein, P38, p-P38, JNK, and p-JNK in neutrophils following treatment with miR-193a<sup>OE</sup>-LEM, miR-NC<sup>OE</sup>-LEM, miR-193a<sup>KD</sup>-LEM, and miR-NC<sup>KD</sup>-LEM. **(E-G)** Protein expression levels of TLR4, p-P38/P38, and p-JNK/JNK were quantified using Image J software. **(H)** Representative immunofluorescence images of N2 neutrophils (Ly6G + Arg-1+) in miR-193a<sup>OE</sup>-LEM, miR-NC<sup>OE</sup>-LEM, miR-193a<sup>KD</sup>-LEM, and miR-NC<sup>KD</sup>-LEM treated group. Scale bars, 50 μm. **(I)** Quantitative evaluation of the findings in **(H)** with a sample size of 3. G1, G2, G3, G4 indicate the miR-193a<sup>OE</sup>-LEM, miR-NC<sup>OE</sup>-LEM, miR-193a<sup>KD</sup>-LEM, and miR-NC<sup>KD</sup>-LEM, respectively. Data represents the mean ± SEM from three separate experiments. ns indicated no significant difference; \**P* < 0.05; \*\**P* < 0.01; \*\*\**P* < 0.001

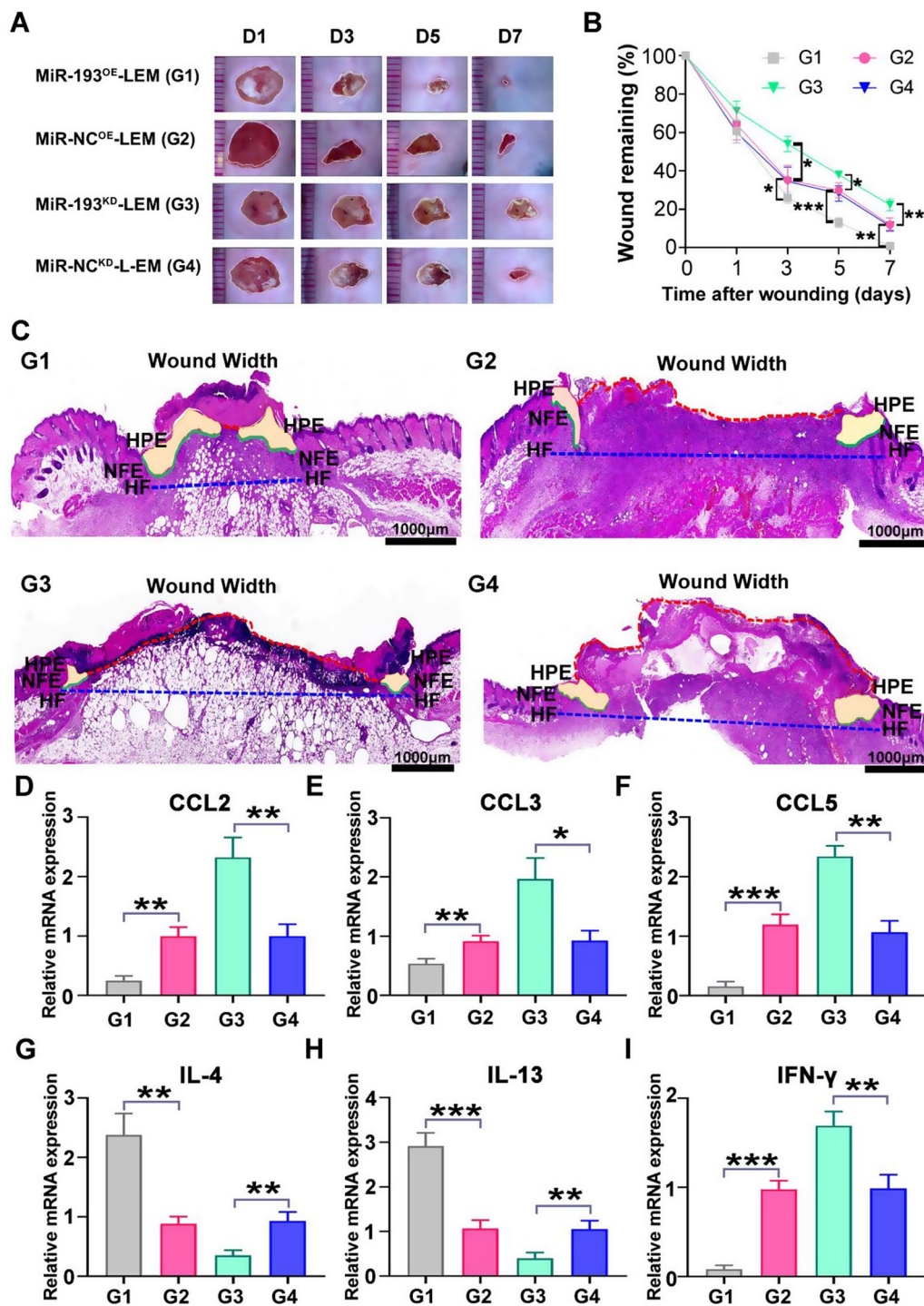


**Fig. 6** miR-193a-5p overexpression in LEM promoted diabetic wound healing and regulated inflammatory environment. **(A)** The gross view of wounds after administration of miR-193a<sup>OE</sup>-LEM, miR-NC<sup>OE</sup>-LEM, miR-193a<sup>KD</sup>-LEM, and miR-NC<sup>KD</sup>-LEM at day 1, 3, 5 and 7. **(B)** Measuring the extent of wound healing in **(A)**. *n* = 3 per group. **(C)** H&E stained sections of miR-193a<sup>OE</sup>-LEM, miR-NC<sup>OE</sup>-LEM, miR-193a<sup>KD</sup>-LEM, and miR-NC<sup>KD</sup>-LEM treated wounds on day 7 displayed morphometric analysis including the newly formed epithelium (NFE, Green line), area of hyperproliferative epidermis (HPE), wound width (Red dotted line), percentage of wound closure (NFE/NFE + wound width × 100%), wound contraction (distance between wound border hair follicles (HF), blue dotted line). **(D-F)** qRT-PCR was used to analyze the levels of chemokines CCL2, CCL3, and CCL5. A sample size of three was used in each group for the experiments, with GAPDH serving as an internal control for normalization. **(G-I)** qRT-PCR was used to analyze the levels of IL-4, IL-13, and IFN-γ cytokines. A sample size of three was used in each group for the experiments, with GAPDH serving as an internal control for normalization. G1, G2, G3, G4 indicate the miR-193a<sup>OE</sup>-LEM, miR-NC<sup>OE</sup>-LEM, miR-193a<sup>KD</sup>-LEM, and miR-NC<sup>KD</sup>-LEM, respectively. Data represents the mean ± SEM from three separate experiments. ns indicated no significant difference; \**P* < 0.05; \*\**P* < 0.01; \*\*\**P* < 0.001

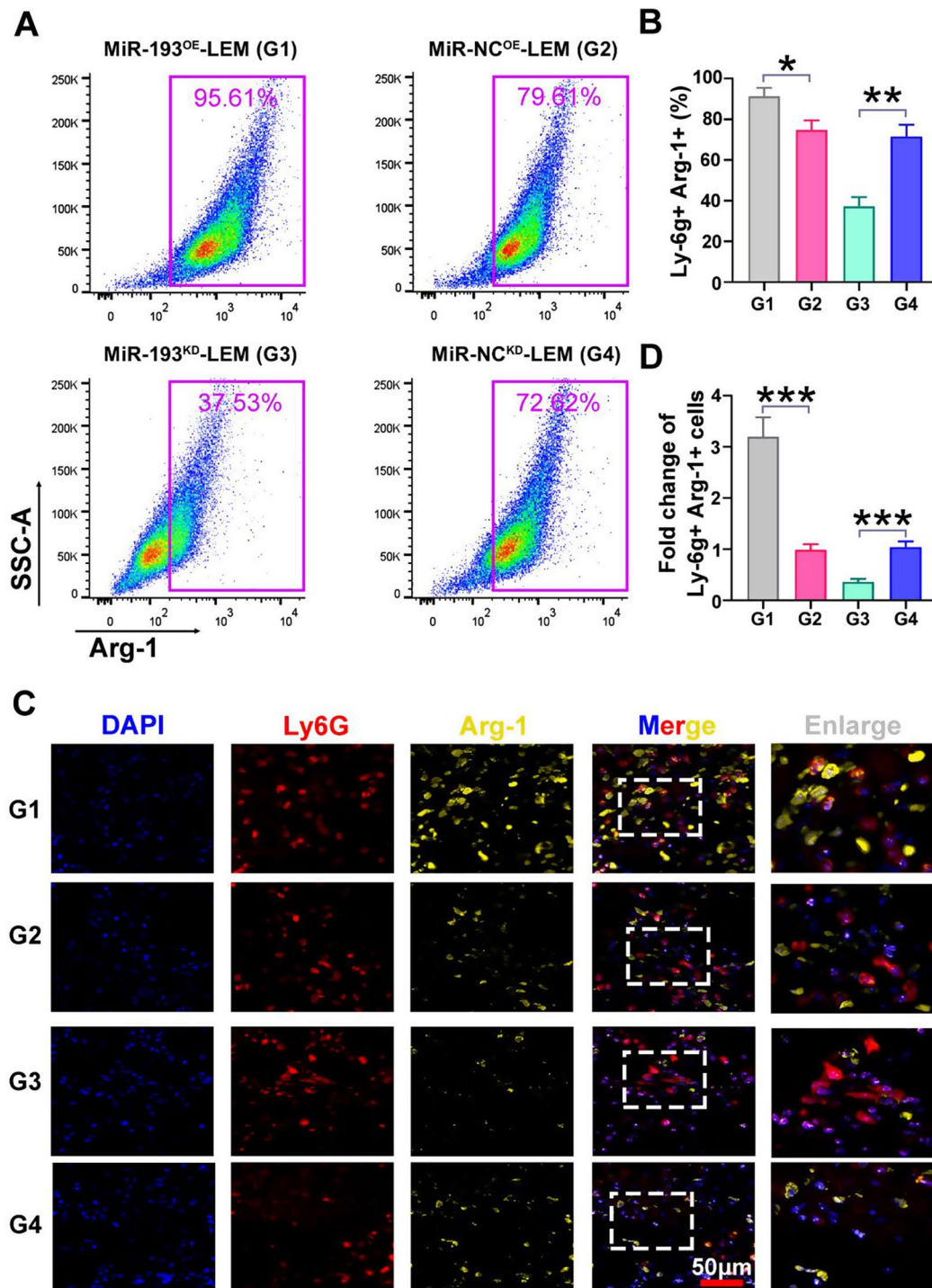


**Fig. 7** miR-193a-5p overexpression in LEM induced N2 polarization during diabetic wound healing. **(A)** Flow cytometry examined the percentage of N2 phenotype neutrophils (Ly-6G + Arg-1+) in diabetic wounds that were treated with miR-193a<sup>OE</sup>-LEM, miR-NC<sup>OE</sup>-LEM, miR-193a<sup>KD</sup>-LEM, and miR-NC<sup>KD</sup>-LEM. **(B)** Quantitative evaluation of the findings from **(A)** with a sample size of 3. **(C)** Representative immunofluorescence images of N2 neutrophils (Ly6G + Arg-1+) in wound sections of miR-193a<sup>OE</sup>-LEM, miR-NC<sup>OE</sup>-LEM, miR-193a<sup>KD</sup>-LEM, and miR-NC<sup>KD</sup>-LEM treated mice. Scale bars, 50 μm. **(D)** Quantitative evaluation of the findings in **(C)** with a sample size of 3. G1, G2, G3, G4 indicate the miR-193a<sup>OE</sup>-LEM, miR-NC<sup>OE</sup>-LEM, miR-193a<sup>KD</sup>-LEM, and miR-NC<sup>KD</sup>-LEM, respectively. Data represents the mean ± SEM from three separate experiments. ns indicated no significant difference; \**P* < 0.05; \*\**P* < 0.01; \*\*\**P* < 0.001

presence of the N2 phenotype compared to the miR-NC<sup>KD</sup>-LEM group, as shown in Fig. 7C. Additionally, quantification of Ly-6G<sup>+</sup>Arg-1<sup>+</sup> cells also showed a similar trend in immunofluorescence analysis (Fig. 7D). The findings further confirmed the beneficial impact of LEM miR-193a-5p on addressing the phenotypic switching deficiency of neutrophils in diabetic wound.

#### LEM overexpressing miR-193a-5p triggered neutrophil metabolic reprogramming in diabetic wound

In our in vitro study, we found that both TLR4/MAPK pathway and mitochondrial metabolism, which is triggered by LEM, play essential role in N2 polarization of neutrophils. To determine the impact of LEM miR-193a-5p in on neutrophils in vivo, we isolated neutrophils from diabetic wounds by using MACS cell sorting kits, checking alterations in the TLR4/MAPK pathway and mitochondrial metabolism (Fig. 8A). Flow cytometry was used to assess the purity of the isolated cell clusters, revealing a high purity of 98.6% based on the MACS Cell Sorting Kit (Fig. 8A). Then, western blot analysis was performed and the results showed that, compared to miR-NC<sup>OE</sup>-LEM treated group, neutrophils from diabetic wounds treated with miR-193a<sup>OE</sup>-LEM had less expression of TLR4 (Fig. 8B and C). However, an opposite result was found following miR-193a<sup>KD</sup>-LEM administration (Fig. 8B and C). We further elucidated the MAPK pathway in metabolic reprogramming in vivo. Expectedly, the results showed that following miR-193a<sup>OE</sup>-LEM treatment, neutrophils from diabetic wounds had less activation of MAPK pathway, with lower phosphorylation of P38 and JNK, whereas neutrophils from miR-193a<sup>KD</sup>-LEM group showed an opposite trend (Fig. 8B, D and E). Additionally, the expression of FAO genes (*Cpt1b*, *Acadm*, and *Acadl*) at the mRNA level were examined in neutrophils isolated from wound tissues after treatment with miR-193a<sup>OE</sup>-LEM, miR-193a<sup>KD</sup>-LEM, and its corresponding controls. As shown in Fig. 8F-H, decreased expression levels of *Cpt1b*, *Acadm*, and *Acadl* were observed in neutrophils from wound site treated with miR-193a<sup>KD</sup>-LEM, and in contrast, utilization of miR-193a<sup>OE</sup>-LEM obviously induced upregulated expression level of these three FAO genes compared to its control group. Furthermore, neutrophils were harvested for further measurement of changes in fatty acid uptake in cell mitochondria. The results suggested that neutrophils mitochondria from miR-193a<sup>OE</sup>-LEM-treated wounds showed enhanced fatty acid uptake, which was characterized by an increased number of green fluorescent aggregates around the mitochondria. However, the miR-193a<sup>KD</sup>-LEM-treated group, showed a lower number of fatty acids around the mitochondria of neutrophils (Fig. 8I). Overall, these findings suggested that miR-193a-5p in LEM can enhance the N2

polarization of neutrophils in diabetic wound healing by inhibiting the TLR4/JNK/P38 MAPK pathway and promoting mitochondrial metabolic reprogramming.

#### Conclusion

Based on the great potential of inflammatory memory in tissue repair, the novel biomimetic nanovesicles for rapid diabetic wound healing were developed in this study. These MNVs, which derived from inflammatory memory activated EpSCs, could rescued the phenotypic switching deficiency of neutrophils in diabetic wounds, stimulating mitochondrial metabolic recalibration and priming neutrophils to a N2 phenotype, finally accelerating diabetic wound regeneration.

In addition to their therapeutic effects, our biomimetic nanovesicles have lots of advantages over other synthetic materials or native EVs, including faster production time, higher yields, good biocompatibility and lower costs [23, 40]. Unlike traditional methods that require cells to secrete vesicles or use expensive EVs-free medium, our MNVs can be produced directly from confluent cells through extrusion. That means they are suitable for large-scale production. It has been reported that the production of MNVs exceeded that of EVs by over 100 times from an equivalent cell count [23]. Furthermore, MNVs can be conveniently freeze-dried and kept as a powder at room temperature for more than 6 months without affecting their physical, morphological, and inherent biological characteristics [41]. Freeze-drying MNVs could eliminate the need for refrigeration and make sample management easier. Furthermore, MNVs applications have lower ethical concerns compared to cell-therapy.

In our work, bioinformatic tools were utilized to analyze the effects of miR-193a-5p overexpression in LEM and recipient neutrophils, revealing that the TLR4/JNK/P38 MAPK signaling pathway is regulated by miR-193a-5p. After being identified as a target of miR-193a-5p through database prediction and dual-luciferase reporter gene assay, the TLR4/JNK/P38 MAPK axis was chosen for additional investigation. Overexpression of miR-193a-5p led to an increase in N2 polarization and a reduction in TLR4 expression and MAPK pathway phosphorylation in neutrophils, indicating the involvement of the miR-193a-5p/TLR4/JNK/P38 MAPK axis in N2 neutrophil polarization.

MiR-193a-5p loaded LEM were used in vivo in diabetic wounds to assess their potential in controlling inflammation and promoting healing. The findings indicated that miR-193a-5p carried by LEM significantly altered the inflammatory conditions in diabetic wounds, induced a shift in mitochondrial metabolism towards N2 polarization, ultimately facilitating re-epithelization and wound healing.

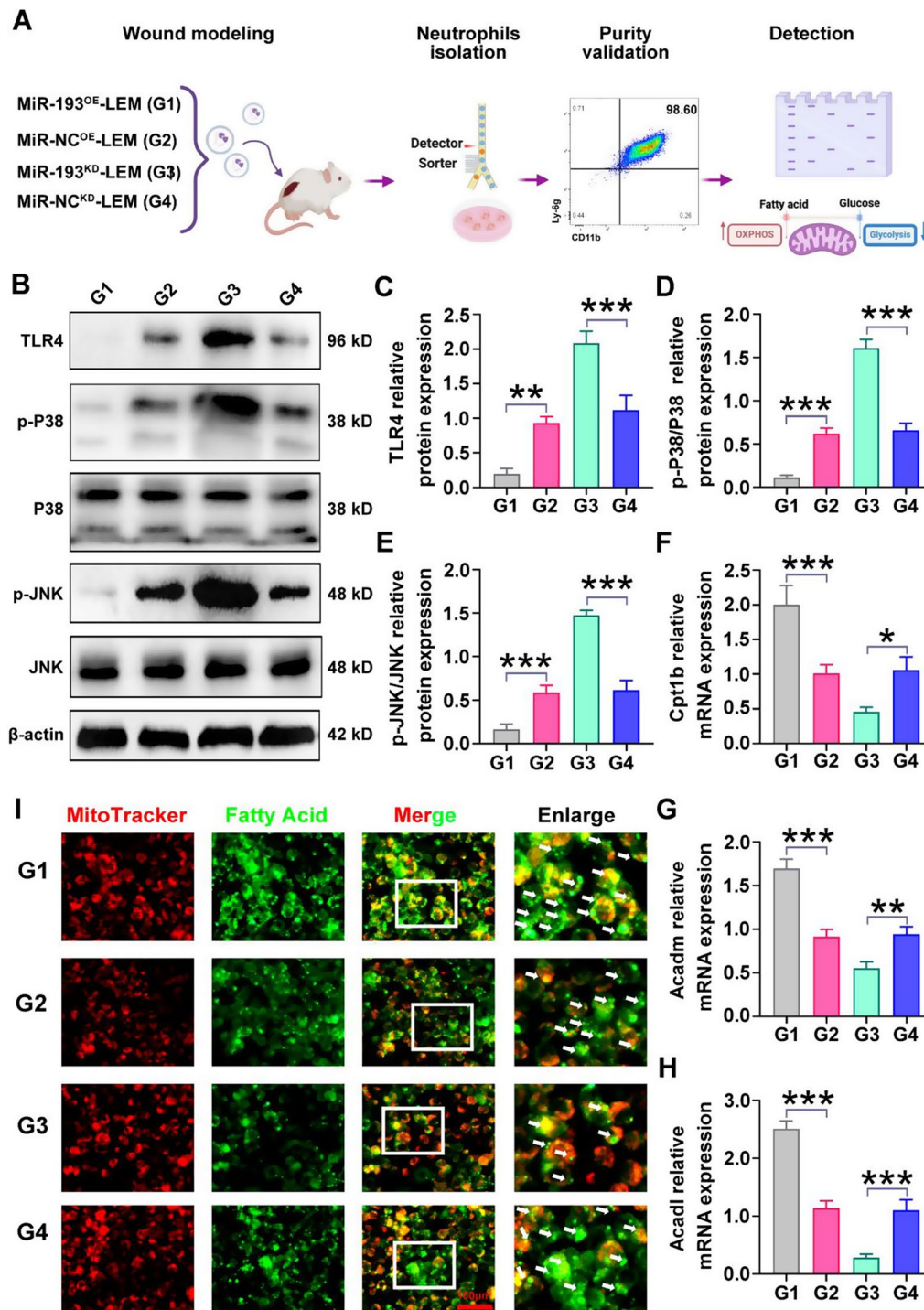


**Fig. 8** LEM overexpressing miR-193a-5p in vivo induced inhibition of TLR4/MAPK pathway and activation of mitochondrial metabolic recalibration. **(A)** A diagram illustrating the experimental process of isolating neutrophils from diabetic wounds using the MACS cell sorting kit and detailing their characteristics. **(b)** Western blot analysis was performed to assess the expression levels of TLR4 protein, P38, p-P38, JNK, and p-JNK in neutrophils isolated from diabetic wounds. **(C-E)** Protein expression levels of TLR4, p-P38/P38, and p-JNK/JNK were quantified using Image J software. **(F-H)** Transcription levels of genes involved in fatty acid oxidation (*Cpt1b*, *Acadm*, and *Acadl*) were measured in neutrophils extracted from diabetic wounds. **(I)** Fatty acid uptake of mitochondria was analyzed in neutrophils isolated from diabetic wounds. Scale bars, 100 μm. G1, G2, G3, G4 indicate the miR-193a<sup>OE</sup>-LEM, miR-NC<sup>OE</sup>-LEM, miR-193a<sup>KD</sup>-LEM, and miR-NC<sup>KD</sup>-LEM, respectively. Data represents the mean ± SEM from three separate experiments. ns indicated no significant difference; \**P* < 0.05; \*\**P* < 0.01; \*\*\**P* < 0.001

Overall, our work emphasized LEM as an efficient bioengineered approach to treating diabetic wound and further identified that miR-193a–5p/TLR4/JNK/P38 MAPK pathway mediated the biological function of LEM by regulating neutrophil plasticity and metabolic reprogramming, which provided a new alternative for wound repair and tissue regeneration. Additionally, while our study primarily focused on the effects of MNVs on neutrophil polarization, the potential influence of MNVs on macrophage polarization towards an M2 phenotype, which is also crucial for wound healing, cannot be discounted. This possibility is supported by the broader implications of the cytokines and chemokines involved, which are known to affect macrophage behavior. Therefore, future research will be directed towards exploring the dual effects of MNVs on both neutrophil and macrophage polarization to gain a comprehensive understanding of their role in wound healing.

#### Abbreviations

AGEs	Advanced glycation end products
CM	Conditioned media
EM	MNVs derived EpSCs
EpSCs	Epidermal stem cells
EpSCs-CM	CM obtained from EpSCs
EVs	Exosome vesicles
FAO	Fatty acid oxidation
HPE	Hyperproliferative epidermis
JNK	c-JUN N-terminal Kinase
LEM	MNVs derived LPS-pretreated EpSCs
L-EpSCs	LPS treated EpSCs
L-EpSCs-CM	CM obtained from L-EpSCs
MACS	Magnetic-activated cell sorting
MAPK	Mitogen-activated protein kinase
MNVs	Mimetic nanovesicles
Mut	Mutant
NETs	Neutrophil extracellular traps
NFE	Newly formed epithelium
OXPHOS	Oxidative phosphorylation
POD	Postoperative day
TEM	Transmission electron microscopy
Treg	Regulatory T
wt	Wild-type

#### Supplementary Information

The online version contains supplementary material available at <https://doi.org/10.1186/s12951-025-03193-5>.

Supplementary Material 1

#### Author contributions

Conceptualization, Y.F., S.J., R.Y.; Data curation, J.Y., Y.X.; Formal analysis, X.Y., H.Z., Y.L.; Investigation, Y.F., J.Y., Y.X.; Methodology, Y.F., J.Y., Y.X.; Project administration, Y.F., J.Y., Y.X.; Supervision, Z.X., S.J., R.Y.; Validation, Z.X., S.J., R.Y.; Visualization, Z.X., S.J., R.Y.; Writing – original draft, Y.F., J.Y., Y.X.; Writing – review & editing, Z.X., S.J., R.Y. All authors have read and agreed to the published version of the manuscript.

#### Funding

This work was financially supported by the National Natural Science Foundation of China (#82373494, #81772138) and Beijing Natural Science Foundation (#7212105).

#### Data availability

No datasets were generated or analysed during the current study.

#### Declarations

##### Ethics approval and consent to participate

The study protocols were reviewed and approved by the Institutional Review Board of Chinese PLA General Hospital.

##### Consent for publication

All authors read and agreed to submit the manuscript.

##### Competing interests

The authors declare no competing interests.

##### Author details

<sup>1</sup>Department of Dermatology, The Seventh Medical Center of Chinese PLA General Hospital, Beijing 100700, China

<sup>2</sup>Chinese PLA Medical School, Beijing 100853, China

<sup>3</sup>Zhujiang Hospital, Southern Medical University or The Second School of Clinical Medicine, Southern Medical University, Guangzhou 510599, China

Received: 23 August 2024 / Accepted: 1 February 2025

Published online: 17 February 2025

#### References

1. Sawaya AP, et al. Deregulated immune cell recruitment orchestrated by FOXM1 impairs human diabetic wound healing. *Nat Commun.* 2020;11(1):4678.
2. Yang L, et al. Biofilm microenvironment triggered self-enhancing photodynamic immunomodulatory microneedle for diabetic wound therapy. *Nat Commun.* 2023;14(1):7658.
3. Graves N, Phillips CJ, Harding K. A narrative review of the epidemiology and economics of chronic wounds. *Br J Dermatol.* 2022;187(2):141–8.
4. Wan L, et al. The advanced glycation end-products (AGEs)/ROS/NLRP3 inflammasome axis contributes to delayed diabetic corneal wound healing and nerve regeneration. *Int J Biol Sci.* 2022;18(2):809–25.
5. Yang J, et al. HucMSC-Exo Induced N2 polarization of neutrophils: implications for angiogenesis and tissue restoration in Wound Healing. *Int J Nanomed.* 2024;19:3555–75.
6. Sansores-España LD, Melgar-Rodríguez S, Vernal R, Carrillo-Ávila BA, Martínez-Aguilar VM, Díaz-Zúñiga J. Neutrophil N1 and N2 subsets and their possible association with Periodontitis: a scoping review. *Int J Mol Sci.* 2022;23(20).
7. Mankan AK, et al. Intracellular DNA sensing by neutrophils and amplification of the innate immune response. *Front Immunol.* 2023;14:1208137.
8. Maus KD, et al. Skewing cPLA(2) $\alpha$  activity toward oxoecosanoid production promotes neutrophil N2 polarization, wound healing, and the response to sepsis. *Sci Signal.* 2023;16(793):eadd6527.
9. Dekoninck S, Blanpain C. Stem cell dynamics, migration and plasticity during wound healing. *Nat Cell Biol.* 2019;21(1):18–24.
10. Shahin H et al. miRNome and proteome profiling of human keratinocytes and adipose derived stem cells proposed miRNA-Mediated regulations of epidermal growth factor and interleukin 1-Alpha. *Int J Mol Sci.* 2023;24(5).
11. Luan J, et al. CD80 on skin stem cells promotes local expansion of regulatory T cells upon injury to orchestrate repair within an inflammatory environment. *Immunity.* 2024;57(5):1071–e867.
12. McCarthy S, Agudo J. Hair care: stem cells control immune response during wound repair. *Immunity.* 2024;57(5):933–5.
13. Naik S, et al. Inflammatory memory sensitizes skin epithelial stem cells to tissue damage. *Nature.* 2017;550(7677):475–80.
14. Cheng D, et al. New insights into inflammatory memory of epidermal stem cells. *Front Immunol.* 2023;14:1188559.
15. Bordon Y. Inflammation. Inflammatory memory is skin deep. *Nat Rev Immunol.* 2017;17(12):731.
16. Larsen SB, et al. Establishment, maintenance, and recall of inflammatory memory. *Cell Stem Cell.* 2021;28(10):1758–e748.
17. Naik S, Fuchs E. Inflammatory memory and tissue adaptation in sickness and in health. *Nature.* 2022;607(7918):249–55.

18. Ryu JS, Kim SY, Kim MK, Oh JY. Inflammation confers healing advantage to corneal epithelium following subsequent Injury. *Int J Mol Sci.* 2023;24(4).
19. Yan B, Lan F, Li J, Wang C, Zhang L. The mucosal concept in chronic rhinosinusitis: focus on the epithelial barrier. *J Allergy Clin Immunol.* 2024;153(5):1206–14.
20. Morroni J, et al. Injury-experienced satellite cells retain long-term enhanced regenerative capacity. *Stem Cell Res Ther.* 2023;14(1):246.
21. Li Y, et al. Exosomes: compositions, biogenesis, and mechanisms in diabetic wound healing. *J Nanobiotechnol.* 2024;22(1):398.
22. Théry C, Amigorena S, Raposo G, Clayton A. Isolation and characterization of exosomes from cell culture supernatants and biological fluids. *Curr Protoc Cell Biol.* 2006;Chap. 3:Unit 3.22.
23. Jang SC, et al. Bioinspired exosome-mimetic nanovesicles for targeted delivery of chemotherapeutics to malignant tumors. *ACS Nano.* 2013;7(9):7698–710.
24. Xiong J, et al. Bioinspired engineering ADSC nanovesicles thermosensitive hydrogel enhance autophagy of dermal papilla cells for androgenetic alopecia treatment. *Bioact Mater.* 2024;36:112–25.
25. Neupane YR, et al. Cell-derived nanovesicles from mesenchymal stem cells as extracellular vesicle-mimetics in wound healing. *Acta Pharm Sin B.* 2023;13(5):1887–902.
26. Jiang Y, Yu M, Song ZF, Wei ZY, Huang J, Qian HY. Targeted delivery of mesenchymal stem cell-derived Bioinspired Exosome-Mimetic nanovesicles with platelet membrane Fusion for atherosclerotic treatment. *Int J Nanomed.* 2024;19:2553–71.
27. Parfejevs V, et al. Injury-activated glial cells promote wound healing of the adult skin in mice. *Nat Commun.* 2018;9(1):236.
28. Liu Y, Tang G, Li J. Long non-coding RNA NEAT1 participates in ventilator-induced lung injury by regulating miR-20b expression. *Mol Med Rep.* 2022;25(2).
29. Allen JE. IL-4 and IL-13: regulators and effectors of Wound Repair. *Annu Rev Immunol.* 2023;41:229–54.
30. Deng Z, et al. TGF- $\beta$  signaling in health, disease, and therapeutics. *Signal Transduct Target Ther.* 2024;9(1):61.
31. Ibrahim A, Yucel N, Kim B, Arany Z. Local mitochondrial ATP production regulates endothelial fatty acid uptake and transport. *Cell Metab.* 2020;32(2):309–19.e7.
32. Dai X, et al. MicroRNA-193a-3p reduces intestinal inflammation in response to Microbiota via Down-regulation of Colonic PepT1. *J Biol Chem.* 2015;290(26):16099–115.
33. Alghetaa H, et al. Resveratrol protects mice against SEB-induced acute lung injury and mortality by miR-193a modulation that targets TGF- $\beta$  signalling. *J Cell Mol Med.* 2018;22(5):2644–55.
34. Han Z, et al. MicroRNA-193a-5p rescues ischemic cerebral Injury by restoring N2-Like Neutrophil subsets. *Transl Stroke Res.* 2023;14(4):589–607.
35. Huang C, et al. MiR-193b-3p-ERBB4 axis regulates psoriasis pathogenesis via modulating cellular proliferation and inflammatory-mediator production of keratinocytes. *Cell Death Dis.* 2021;12(11):963.
36. Soeda N, et al. Plasma exosome-encapsulated microRNA-21 and microRNA-92a are promising biomarkers for the prediction of peritoneal recurrence in patients with gastric cancer. *Oncol Lett.* 2019;18(5):4467–80.
37. Chen JJ, et al. Ribonuclease T2 from *aspergillus fumigatus* promotes T helper type 2 responses through M2 polarization of macrophages. *Int J Mol Med.* 2020;46(2):718–28.
38. Du P, et al. Saikosaponin-d attenuates Hashimoto's thyroiditis by regulating macrophage polarization. *J Immunol Res.* 2022;2022:7455494.
39. Li S, Yang P, Ding X, Zhang H, Ding Y, Tan Q. Puerarin improves diabetic wound healing via regulation of macrophage M2 polarization phenotype. *Burns Trauma.* 2022;10:tkac046.
40. Lin M, et al. Immunosuppressive microvesicles-mimetic derived from tolerant dendritic cells to target T-lymphocytes for inflammation diseases therapy. *J Nanobiotechnol.* 2024;22(1):201.
41. Neupane YR et al. Lyophilization preserves the intrinsic cardioprotective activity of Bioinspired Cell-Derived nanovesicles. *Pharmaceutics.* 2021;13(7).

#### Publisher's note

Springer Nature remains neutral with regard to jurisdictional claims in published maps and institutional affiliations.